Simulations of the implosion and stagnation of compact wire arrays

C. A. Jennings,[1] M. E. Cuneo,[1] E. M. Waisman,[1] D. B. Sinars,[1] D. J. Ampleford,[1] G. R. Bennett,[1] W. A. Stygar,[1] and J. P. Chittenden[2]
[1]*Sandia National Laboratories, Albuquerque, New Mexico 87185-1106, USA*
[2]*The Blackett Laboratory, Imperial College, London SW7 2BW, United Kingdom*

(Received 31 March 2010; accepted 12 July 2010; published online 24 September 2010)

Wire array z-pinches have been used successfully for many years as a powerful x-ray source, as a dynamic hohlraum, and as an intense K-shell radiation source. Significant progress has been made in the effective modeling of these three-dimensional (3D) resistive plasmas. However, successful modeling also requires an accurate representation of the power delivered to these loads from the generator, which is an uncertainty potentially as large as the magnetohydrodynamic (MHD) implosion dynamics. We present 3D resistive MHD simulations of wire arrays that are coupled to transmission line equivalent models of the Z generator, driven by voltage sources derived directly from electrical measurements. Significant (multi-mega-ampère) current losses are shown to occur in both the convolute and the final feed. This limits the array performance and must be correctly accounted for to accurately represent the generator response to the load. Our simulations are validated against data for compact: 20 mm diameter, 10 mm long wire arrays that have produced the highest x-ray power densities on Z. This is one of the most comprehensive experimental data sets for single and nested wire arrays and includes voltage, current, x-ray power and energy, and multiple mass distribution measurements. These data tightly constrain our simulation results and allow us to describe in detail both the implosion and stagnation, and how energy is delivered to, and radiated from z-pinch loads. We show that the radiated power is consistent with the kinetic energy delivered to a distributed 3D mass profile over its implosion and stagnation. We also demonstrate how the local inductance of the transmission line connecting to the wire array is responsible for delivering more than 50% of the total radiated power. This makes the power output dependent on the design of specific elements of the generator, and their response to the imploding load, and not just on the peak current that can be delivered. © *2010 American Institute of Physics*. [doi:10.1063/1.3474947]

I. INTRODUCTION

A wire array z-pinch is formed of a cylindrical array of fine metallic wires to which a current is applied, driving a cylindrically convergent implosion. Compact wire arrays consisting of 300 tungsten wires, arranged around a 2 cm diameter and imploded on the Z generator of Sandia National Laboratories, have routinely produced x-ray powers in excess of 100 TW from a ~20 MA drive current rising in ~100 ns. Well optimized versions of this class of array have demonstrated powers of 200–250 TW, making these sources a potentially attractive driver for inertial confinement fusion.[1] Wire arrays have additionally found applications as high intensity K-shell sources, and dynamic hohlraums used in radiation flow experiments. To achieve the ~PW powers required for proposed fusion schemes[2] and to further advance and optimize sources for other applications requires a detailed understanding of exactly how x-ray power is generated in the stagnating z-pinch. This, in turn, requires us to understand both how effectively the generator couples current to these loads and how this coupling responds to the evolving z-pinch.

In this work, we validate a three-dimensional resistive magnetohydrodynamic (MHD) code against a broad range of experimental measurements characterizing the evolution of different masses of single compact wire arrays. We demonstrate that results are consistent with an additional current loss associated with the transmission line section that drives the array. We use the electrical diagnostics of the generator and our validated MHD code to determine the magnitude of this current loss and more accurately assess the electrical power coupled to the z-pinch load. Previous analysis has indicated that the effective mean radius of the current trails significantly behind the main implosion[3] to remain well outside the brightest emitting regions as the plasma stagnates on the array axis. However, we show how the presence of a current loss is consistent with the current more closely following the observed implosion trajectory. We further demonstrate that when we account for the distributed mass profile created by the development of implosion instabilities, the energy radiated in the main x-ray pulse from the stagnating wire array is consistent with the total kinetic energy delivered by magnetic work done accelerating the imploding plasma. These results are consistent with those of Peterson *et al.*[4] and Lemke *et al.*[5] and do not require additional resistive, viscous, or compressional heating processes to explain the energy radiated or the final pinch radius reached. Finally, we discuss how the radiated energy depends on the specific response of the generator to the imploding array and indicate how this coupling may be modified or optimized for specific applications.

This paper is arranged as follows. In Sec. II, we briefly describe the Z generator and how the resistive MHD code GORGON (Ref. 6) is set up to model the implosion and stag-

 © 2010 American Institute of Physics

Downloaded 18 Jan 2011 to 134.253.26.11. Redistribution subject to AIP license or copyright; see http://pop.aip.org/about/rights_and_permissions

nation of wire array z-pinches. In Sec. III, we describe how electrical measurements combined with the known architecture of the Z generator may be used to construct a voltage drive for wire array load simulations. These simulations drive a current at the z-pinch that is consistent with this voltage and our MHD description of the load. This is seen to be less than the current measured to leave the convolute at a radius of ~5.8 cm, implying a current loss in between the convolute and the array that has not been directly diagnosed. In Sec. IV, we validate our MHD description against numerous experimental measurements for three different masses of compact wire array loads, demonstrating good agreement between simulated and measured quantities. Section V compares different interpretations of this current loss, demonstrating that it may represent either a loss of current in the power feed or trailing current within the array volume. We show that results and simulations are inconsistent with current, trailing significantly behind the imploding mass, and strongly indicative of an undiagnosed current loss in the transmission line feeding the array. Section VI then analyzes in more detail the delivery of energy to an imploding z-pinch, demonstrating x-ray production to be consistent with the kinetic energy supplied to the imploding array, without the need to invoke any additional heating mechanisms in the stagnated plasma. Finally, Sec. VII discusses in more detail how the generator couples energy to the load and then responds to its implosion.

II. SIMULATING WIRE ARRAYS ON THE Z GENERATOR

While z-pinch experiments continue to be conducted at a number of different facilities, this work focuses on the implosion of compact tungsten wire arrays on Sandia National Laboratories Z generator.

A. Simulation setup

Array simulations were performed by the three-dimensional (3D) resistive MHD code GORGON,[6] developed at Imperial College, London and at Sandia National Laboratories.[7] All of the compact tungsten wire arrays discussed and modeled here are 300 wire cylindrical arrays 2 cm in diameter and 1 cm in height, which were fielded at three different total masses (1.1, 2.5, and 6 mg). All of the calculations discussed model the full height and full circumference of these loads at a fixed 120 μm spatial resolution. The discrete wires of these arrays are initialized as cold dense vapor in which the initial ionization state is suppressed above a density of 10 Kg m^{-3} to allow the formation of the core-corona ablation structure experimentally observed.[8] This technique has been repeatedly used to successfully model the initial discrete wires, without the need to model the complex phase transitions involved in allowing the wires to evolve from metal to plasma.[9] To each initial wire we apply a 10% sinusoidal mass perturbation randomly modulated in phase and amplitude. This accounts for the redistribution of mass arising from an ablation instability that has been successfully modeled with this code,[9] but for which we lack the resolution to self-consistently evolve in these calculations. The same initial perturbation setup is used for all of the calculations we discuss here, with no additional parameters varied between simulations. To ease resolution requirements, the initial array mass is distributed between 120 discrete wires, rather than the 300 fielded in the experiment. The magnetic field is set on a circular boundary 2 mm outside the initial array radius, with the load voltage monitored at this location and used to couple our computational domain to a transmission line representation of the Z generator. Proposed by Stygar *et al.*,[10] this coupling of a 3D MHD code to a realistic representation of the generator allows us to simultaneously study both the array physics and the generator coupling. Since these x-ray sources are magnetically driven, accurately assessing how the current is delivered and the voltage is maintained is crucial to accurately representing how the radiation is produced.

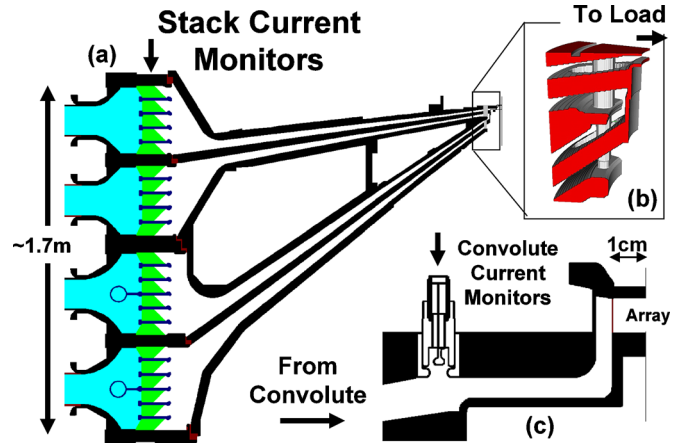

FIG. 1. (Color online) (a) Vacuum/water insulator stack connecting water transmission lines to vacuum magnetically insulated transmission lines, which connect to the (b) convolute, which connects to the (c) load. The location of stack and convolute current monitors is shown.

B. The Z generator

For reference, the architecture of the center section of the Z generator prior to its recent refurbishment is shown in Fig. 1.[11–13] Water transmission lines couple to a water/vacuum insulator stack which drive four vacuum magnetically insulated transmission lines (MITL) (a). These lines are coupled together through a double post hole convolute (b) that connects to a short final transmission line feeding the wire array load region (c). Current and voltage monitors in the insulator stack monitor the power entering the vacuum section, with further current monitors recording the current halfway down these lines. Additional current monitors are located just inside the convolute at the start of the final transmission line feeding the load.[14] In this work, we refer to this measurement as the convolute current, although in other works it has also been referred to as the inner MITL current. Measurements at the water/vacuum insulator stack are referred to as the stack current or voltage. The current actually flowing in the wire array will be referred to as the load current to differentiate it from the convolute current measured ~5.8 cm from the actual load region. Previous analysis of wire arrays on this machine have referred to the convolute

Downloaded 18 Jan 2011 to 134.253.26.11. Redistribution subject to AIP license or copyright; see http://pop.aip.org/about/rights_and_permissions

TABLE I. References describing different aspects of wire array evolution.

Data type	Reference
Trajectory	2, 3, and 17
Mass ablation	18
Mass profile	19 and 20
Radiated power and energy	20 and 21
Electrical data	21–23

current as the load current under the assumption that no current is lost beyond this point. Comparison of the convolute current measurement with stack measurements indicate a multi-mega-ampère (multi-MA) current loss attributed to the convolute and described extensively in the literature.[15,16] In this work, we infer an additional multi-MA current loss in the transmission line connecting the convolute and the load region which we will refer to as the feed loss.

C. Data on wire array implosions

Compact wire arrays were fielded on Z for many years preceding its refurbishment. An extensive data set was accumulated during this time, diagnosing nearly every aspect of the wire array implosion and providing an extremely valuable resource in validating multiple aspects of a wire array simulation. Examples of the data and analysis used in this work, and the aspect of wire array evolution they describe, are briefly summarized in Table I.

III. VOLTAGE DRIVE

Given we have simultaneous measurements of the current and voltage at the vacuum water insulator stack, we can accurately assess the power entering the vacuum section. Since we know the impedance profiles of the four vacuum transmission lines that feed the convolute, we can use these measurements to reconstruct the voltage seen at the convolute under the assumption that the transmission lines behave as ideal, lossless transmission lines. Procedures for reconstructing the convolute voltage under this assumption were first described by Cuneo *et al.*[3] and are also detailed in Refs. 7 and 23. The assumption of an ideal, lossless transmission line prior to the convolute is reasonable if magnetic insulation is established early in the current pulse and if current loss resulting from electron flow in the lines is localized to the convolute. Furthermore, this assumption requires that electrode plasmas do not close the feed gaps over the course of the experiment. Given ~ 1 cm feed gaps at the entrance to the convolute[24] and assuming a cathode plasma expansion velocity of ~ 2.5 cm/μs,[11] these feed lines will not close and the change in the vacuum impedance of the line will be negligible at this location for the ~ 100 ns duration of the experiment. Since each of the four transmission lines independently monitor the voltage and current at the insulator stack, we can separately translate measurements for each line to construct the convolute voltage, and average them under the assumption that the inductance separating the lines at the convolute is small compared to the inductance of the load

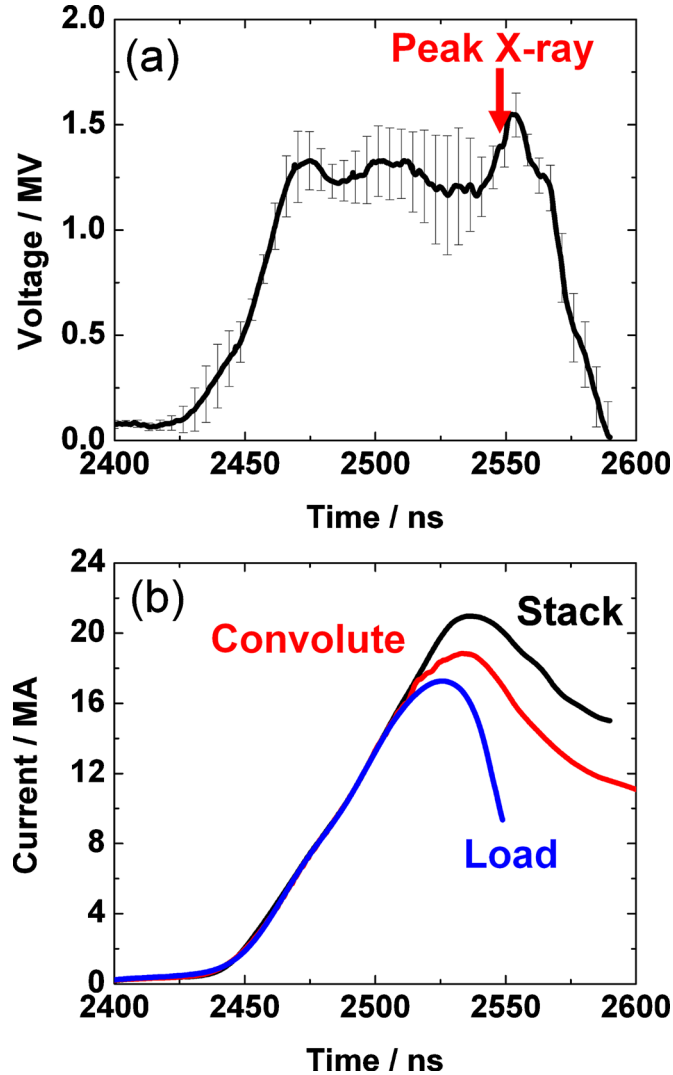

FIG. 2. (Color online) (a) Average convolute voltage reconstructed from insulator stack measurements for a 6 mg compact array implosion. Error bars denote standard deviation between four lines. (b) Corresponding currents measured at the insulator stack and convolute, and inferred at the load for Z shot 1098.

region after the convolute. An example of the convolute voltage calculated in this way is shown in Fig. 2(a) for a 6 mg compact tungsten array imploded on the Z generator and discussed later in Sec. IV. The error bars denote the standard deviation between the different line measurements. This convolute voltage measurement now derives from voltage and current probe measurements translated down feed lines that differ significantly in their inductance and capacitance. The close agreement between these constructed voltages therefore gives us some confidence in this measurement.

This measurement represents the voltage at the convolute, and so represents the voltage at the start of the final feed section leaving the convolute. Any current loss located within the convolute will appear in parallel with this final feed section, and so be driven by the same voltage. We can therefore use this voltage measurement to directly drive a transmission line representation of the final feed, coupled to our resistive MHD code calculation. For the specific wire array implosion for which this voltage was constructed, the

Downloaded 18 Jan 2011 to 134.253.26.11. Redistribution subject to AIP license or copyright; see http://pop.aip.org/about/rights_and_permissions

current that flows through the feed and load calculation will now be consistent with the measured convolute voltage. Assuming our wire array load calculation is accurate, any current losses in the vicinity of the convolute do not have to be explicitly accounted for as they are simply driven by the same voltage. Figure 2(b) shows the actual current in the 6 mg tungsten load inferred in this way from the convolute voltage for that shot. For comparison, we also show the insulator stack and convolute current measurements, indicating that the actual drive current is considerably less than the convolute current measurement taken at the start of the final feed to the load.[7] This implies that there is an additional current loss downstream of this current measurement that must be accounted for. Such a current loss has previously been proposed as a plausible explanation for the discrepancy between measured and simulated load currents in wire array simulation work performed by Peterson *et al.*[25] Additional current losses have also been applied in simulations of magnetically driven flyer plates on the Z generator performed by Lemke *et al.*;[26] however, now we are able to infer a loss consistent with electrical voltage measurements. Inferred in this way, such a current loss is assumed to also be in the vicinity of the convolute, inside of the convolute current measurement. A comparable loss would, however, still be required if it were located closer to or within the load region. We consequently cannot, at this stage, differentiate between a current loss in the final feed and a current path in the array volume that has not been accounted for in our load calculation.

IV. VALIDATION OF MHD LOAD DESCRIPTION

The use of voltage measurements to analyze the current delivery to the load and infer a current loss implicitly assumes that our 3D resistive MHD code produces an accurate representation of a wire array implosion. To verify this, it is important that we validate our model of the imploding wire array against available experimental measurements to help ascertain the exact nature of this current loss. To accomplish this, we apply our model to a number of differently massed compact tungsten single wire array loads. For each shot, we calculate a convolute voltage from the electrical data specific to that shot and then use this to drive our calculations. Since the convolute voltage differs significantly between different array implosions, this method will not provide a predictive capability, but it does provide a current consistent with the generator measurements and our MHD description of the load. It therefore allows us to validate our description of the load without the need to quantitatively model any of the current losses, and without introducing the uncertainties resulting from such an attempt.

The evolution of wire arrays is well-understood to be divided into the three phases of ablation, implosion, and stagnation.[27] Early in time, the current drives the ablation of the discrete array wires. Material ablates with an approximately constant velocity and streams toward the array axis.[8] During this time, ablation instabilities redistribute some of the wire mass, resulting in an axial perturbation.[9,28,29] When the wires eventually run out of mass, the applied current

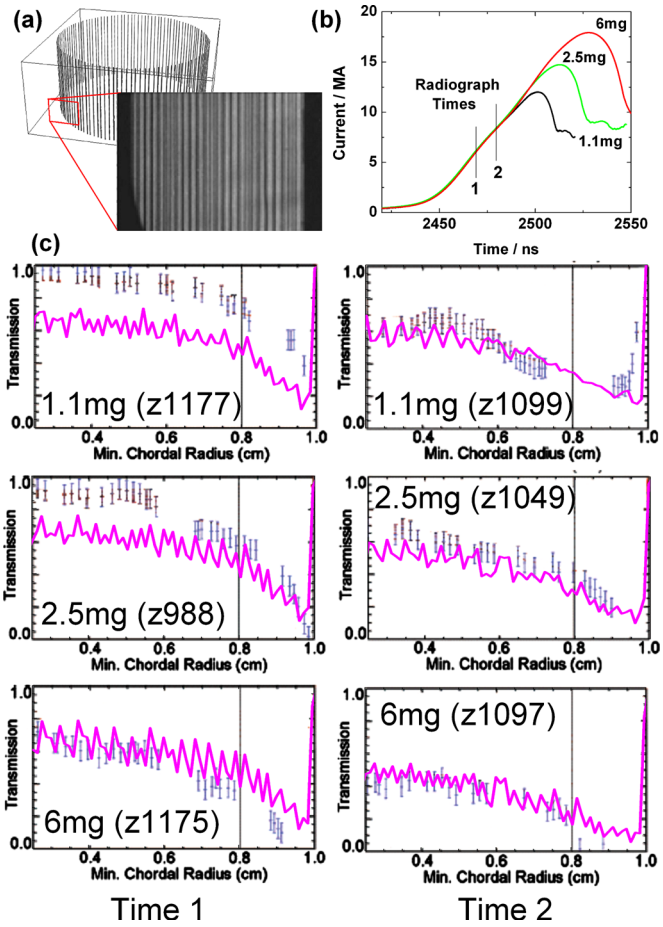

FIG. 3. (Color online) (a) Example radiograph from which transmission was calculated. (b) Radiographs timing with reference to current pulses. (c) Comparison of measured and simulated transmission. Data were reported by Sinars *et al.* (Ref. 18).

drives the cylindrically convergent implosion of a plasma shell that accretes the mass originally ablated. Magneto–Rayleigh–Taylor (MRT) instabilities[30] seeded by the ablation instability grow as the implosion proceeds, significantly disrupting the uniformity and dramatically increasing the width of the imploding shell. Finally, this shell stagnates on the array axis, thermalizing the kinetic energy built up during the implosion and radiating this energy as x rays. An extensive experimental data set exists for compact tungsten wire arrays, including quantitative density measurements, convergence ratios, x-ray power pulses, implosion trajectory measurements, and the electrical voltage and current diagnostics. This comprehensive data set allows us to validate each phase of the wire arrays evolution.

A. Ablation

To characterize the ablation of the array material Sinars *et al.*[18] have presented a series of measurements of mass ablated from the wires to fill the array volume. Radiographs were taken of these arrays at early times prior to the onset of implosion. An example radiograph is shown in Fig. 3(a) where the discrete array wires are still visible. The transmission of x rays through the ablated mass from a 1.865 keV backlighting source was measured by looking between the

Downloaded 18 Jan 2011 to 134.253.26.11. Redistribution subject to AIP license or copyright; see http://pop.aip.org/about/rights_and_permissions

discrete wires, and these results are shown in Fig. 3(c). Measurements are shown for the three different array masses at two times during the ablation phase, marked by the drive current reaching ~6 and ~8 MA. To compare with simulations, we use density and temperature dependent tungsten opacities applicable to our array parameters and also presented by Sinars *et al.*[18] as part of this experimental data set. Using the simulated densities and temperatures with these opacities, we calculate the attenuation of the radiography x-ray source along lines of sight through our computational volume. The transmission coefficient calculated in this way provides an integrated measure of the mass along these lines of sight. These results are compared to the experimentally measured transmissions in Fig. 3(c). For reference, Fig. 3(b) marks the approximate time of these measurements relative to the simulated currents for the three array masses. We obtain excellent agreement between these measurements for all three masses at the later time. At the earlier time, we obtain excellent agreement for the 6 mg array and reasonable agreement for the 2.5 mg array. For the 1.1 mg array, our calculations appear to overestimate the ablation rate, although at the later time, agreement is recovered. This indicates there is an effect of the ablation physics not recovered in our calculations. The principal change between these arrays is the total array mass which is changed by using different initial wire sizes. This is likely to affect the ratio between the wire core size and the interwire gap which is known to affect the ablation rate.[8] It is therefore not surprising that we do not recover this effect in our calculations. Since our model maintains the same resolution and wire number, and since wires are initialized as columns of material one computational cell wide, our effective gap to core size ratio is determined by our resolution. As such, it does not vary as the array mass varies, as demonstrated by the consistent transmission (hence ablation rate) maintained between the calculations of the different masses. While this does highlight an issue that requires further investigation, it only results in a discrepancy for the lightest array mass and this discrepancy does not persist to later times. As such, we can have some confidence that our model is able to reasonably capture the ablation physics and resulting density profile and certainly capture it very well for the heavier 6 mg arrays.

B. Implosion

Continuing through into the implosion, a series of 6.151 keV radiographs are available, providing quantitative measurements of density distributions during the implosion. Abel inversion of these density measurements is able to recover the density distribution as a function of radius for the imploding plasma.[20] Four such radiographs and density measurements are shown is Fig. 4, charting the evolution of the imploding density for the 2.5 mg array up until ~5 ns prior to stagnation.[19] For comparison, the density distribution of the 1.1 mg array is also shown ~4 ns prior to stagnation.[20]

Figure 4(a) is a radiograph of a 2.5 mg load where a second wire array was concentrically nested within the first. The discrete wires of the inner array are still visible, but since the imploding material has not yet reached this location, the central section of the image was removed prior to the Abel inversion. This did result in a 30% reduction in the total Abel inverted mass, so the density distribution was then renormalized to the total mass of the outer array, allowing this measurement to characterize the implosion of a single 2.5 mg wire array. Excellent agreement is obtained between the simulated and measured density distributions for Figs. 4(a) and 4(c) of the 2.5 mg array implosion, and Fig. 4(d) of the 1.1 mg array. Figure 4(b) disagrees, but this radiograph had a factor of 2 lower contrast ratio, with the integrated mass being ~20% low. The azimuthally uniform assumption of the Abel inversion was also potentially invalidated by a prominent bubble feature seen in this image.

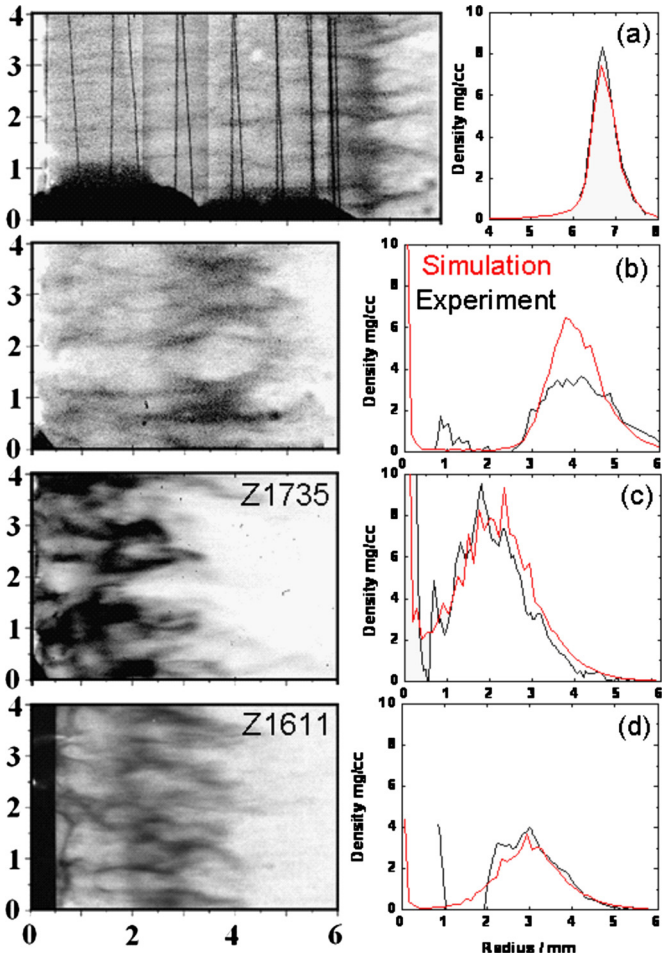

FIG. 4. (Color online) (a)–(c) Radiographs charting the implosion of a 2.5 mg array. Experiments were by Cuneo *et al.* (Ref. 19). (d) Radiograph of a 1.1 mg array implosion, reported by Sinars *et al.* (Ref. 20).

In addition to radiography, further information on the trajectory of the implosion is available from radial optical streak images, x-ray pinhole camera images, and laser shadowgraphy. These measurements are described by Cuneo *et al.*[3,17] and compared to our simulated implosion trajectories in Fig. 5. The simulated quantity we compare to is the radial position of the center of mass as a function of time. To provide some indication of the width of the imploding mass distribution, we also include the implosion trajectory of the inner radius containing only 25% of the total array mass and the radius of the outer edge enclosing 90% of the array mass.

Downloaded 18 Jan 2011 to 134.253.26.11. Redistribution subject to AIP license or copyright; see http://pop.aip.org/about/rights_and_permissions

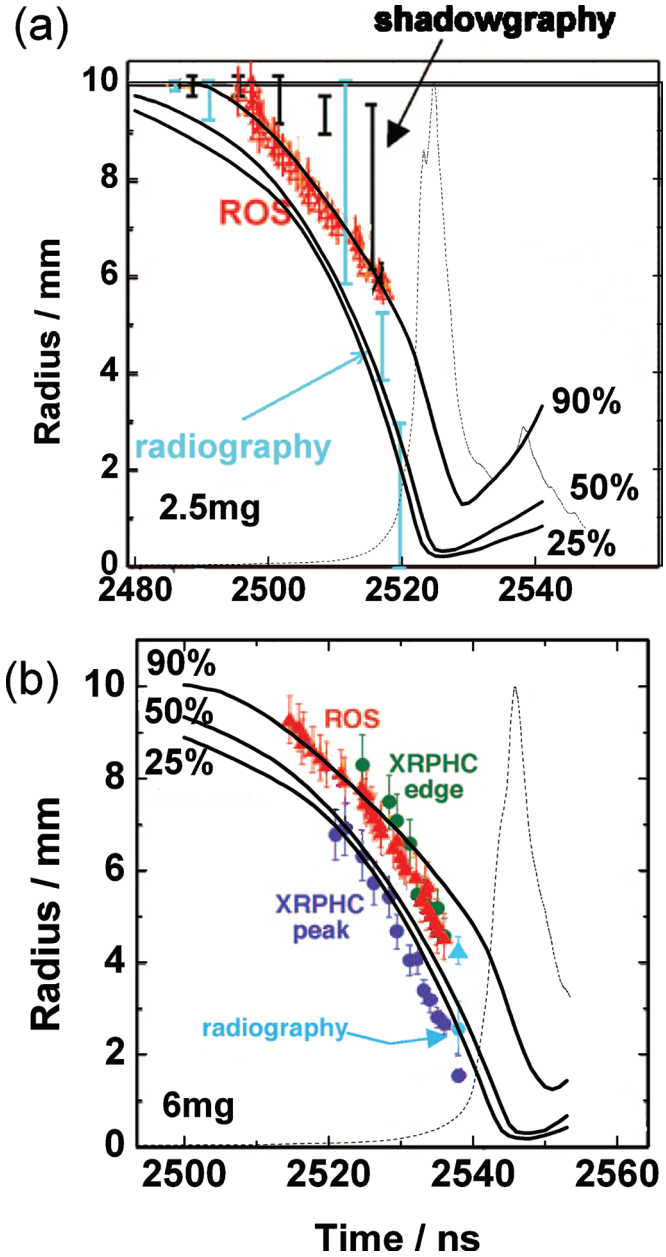

FIG. 5. (Color) Implosion trajectories of a (a) 2.5 and (b) 6 mg array. Black lines: radius containing 25%, 50%, and 90% of array mass. The dotted line is normalized x-ray power. Experimental data for radial optical streak (ROS), x-ray pinhole camera (XRPHC), and radiography, reported by Cuneo *et al.* (Ref. 3).

For both the 6 and 2.5 mg array implosions, the trajectory measured from the radial optical streak agrees with the trajectory of the outer surface of the imploding mass as suggested in Refs. 3 and 17. For the 2.5 mg array, the peak emission measured with an axial x-ray pinhole camera agrees with the leading edge of the implosion, indicating that the radiation is predominantly emitted from the front of the implosion surface as it accretes the ablated mass that fills the array volume. Radiographic data are encompassed by these limits, consistent with this measurement representing the bulk of the imploding mass. Shadowgraphy measurements appear to lag behind the main implosion, consistent with this diagnostic monitoring the lowest density material trailing far behind the main implosion.

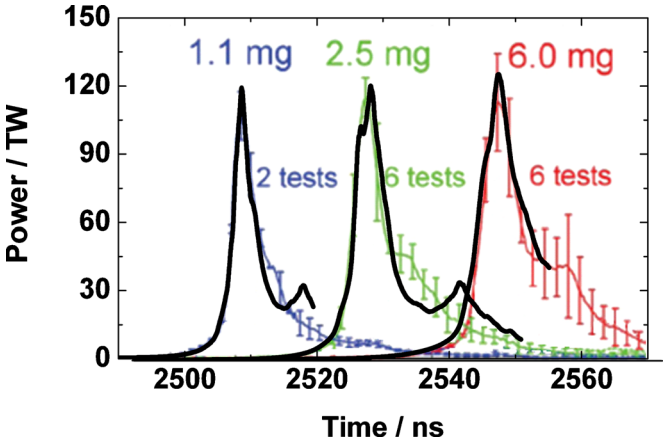

FIG. 6. (Color online) Simulated and measured x-ray powers for mass scan. Timing was adjusted on simulated powers to compare pulse shape and magnitude. Experimental data were reported by Sinars *et al.* (Ref. 20).

C. Stagnation

Continuing to stagnation and x-ray production, Fig. 6 compares the simulated x-ray powers with those measured for these loads and presented by Sinars *et al.*[20] Error bars in the measurements denote the variation between multiple shots, with the simulated x-ray powers seen to agree to within the shot to shot variation. For comparison to magnitudes and pulse shapes, the simulated pulses have been time shifted to the experimental times by a few nanoseconds and other comparisons to experiment are relative to this peak x-ray time. The final convergence ratios reached by the imploding arrays were also measured for these shots at peak x-ray power. Figure 7(a) shows a simulated convergence ratio assessed by integrating the radiation emitted along a line of sight through the array volume and measuring the average width containing 50% of that emission. This is essentially the same measure used to experimentally assess the convergence ratio from pinhole camera imaging and streaked grazing incidence camera images detailed by Sinars *et al.*[20] We show two calculated measurements: the first assumes a completely optically thin plasma and the second allows attenuation by a locally calculated opacity which reduces emission from the dense central section of the stagnating pinch, resulting in a broader width. Figure 7(b) compares these measurements to the convergence ratio reached by the azimuthally averaged current distribution, monitoring a radius containing 75% of the total current. The simulated convergence ratios are found to be in general agreement with those measured. The optically thin measurement of the emitting region is found to disagree significantly for the heaviest 6 mg arrays for which opacity effects are likely to be most significant. In each of the simulations, the current is seen to converge to its minimum radius after peak x rays, indicating that it trails the main implosion.

Simultaneous agreement among the simulated mass profiles, x-ray powers, and convergence ratios is obtained by requiring agreement with the reconstructed convolute voltage. The current loss inferred using this method for these shots is demonstrated in Fig. 8. At peak x rays, the discrepancy between the measured convolute current and the "true"

Downloaded 18 Jan 2011 to 134.253.26.11. Redistribution subject to AIP license or copyright; see http://pop.aip.org/about/rights_and_permissions

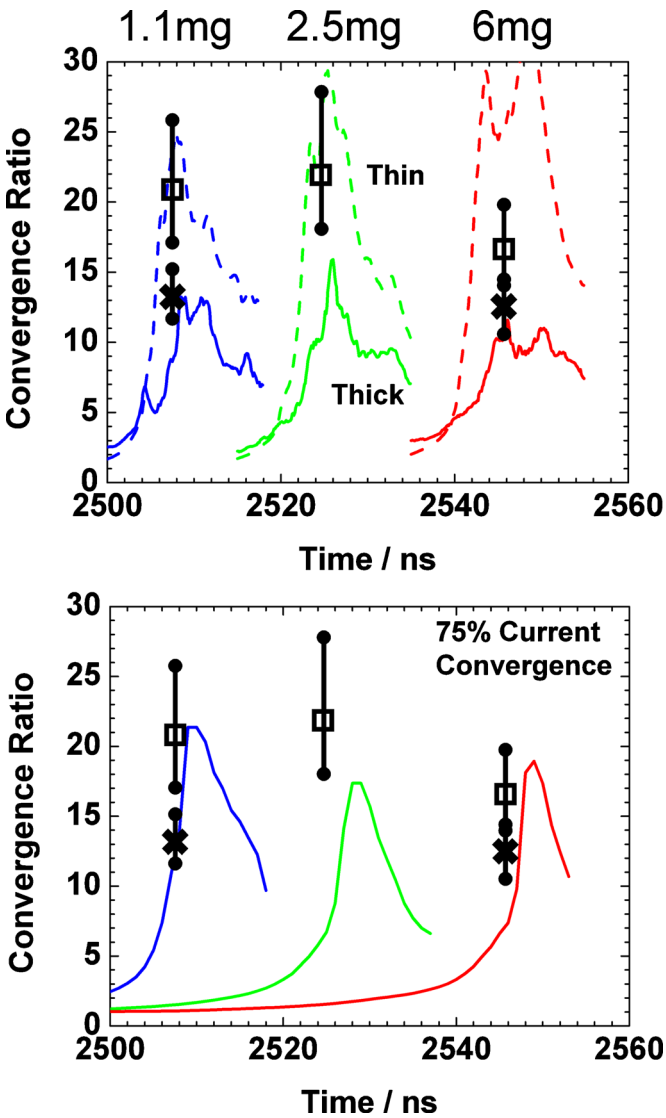

FIG. 7. (Color online) (a) Simulated convergence ratio measuring radius containing 50% of total emission, compared to the same width measured from pinhole camera images (squares) or streaked grazing incidence camera (cross). (b) Convergence ratio of radius containing 75% of the azimuthally averaged current. Experimental convergence were reported by Sinars *et al.* (Ref. 20).

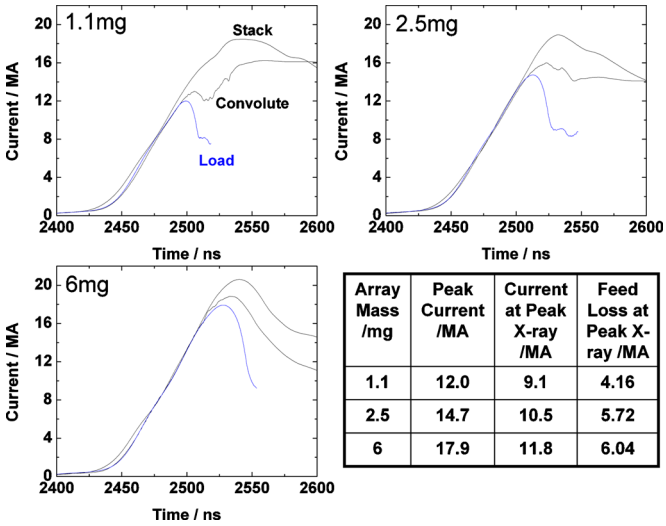

Array Mass /mg	Peak Current /MA	Current at Peak X-ray /MA	Feed Loss at Peak X-ray /MA
1.1	12.0	9.1	4.16
2.5	14.7	10.5	5.72
6	17.9	11.8	6.04

FIG. 8. (Color online) Current measured at the insulator stack, at the convolute, and the load current, consistent with the calculated convolute voltage and the MHD model for mass scan. The table shows load currents and losses at representative times.

load current is seen to increase from 4.1 MA with the 1.1 mg array to 6.0 MA with the 6 mg. This would seem to indicate an increase in the degree of current loss with increasing mass and implosion time, despite the fact that these longer implosion times are generating a lower voltage with which to drive this loss. The convolute current monitor for the 1.1 mg implosion also demonstrates a large increase in current shortly after stagnation, which is consistent with a short circuit forming in the power feed.

V. CURRENT LOSS VERSUS TRAILING CURRENT

Using the electrical diagnostics, one additional measure of the implosion trajectory is available. Assuming negligible resistance associated with the feed and load, we can integrate the convolute voltage to obtain a measure of LI as a function of time, where L is the total inductance of the feed section and wire array, and I is the current that flows through this assembly. Since we know the inductance of the feed, we can assume this inductance remains constant and recover the inductance of the wire array load region as a function of time. Assuming the current flows in an imploding thin cylindrical shell, we can recover from this inductance the implosion trajectory of the current radius. This method of unfolding the inductance has been used extensively in the analysis of wire array implosions.[3,17,22] This method does of course assume we know what current is flowing within the array volume contributing to the load inductance, and ambiguity over this is the very current loss problem discussed earlier. We do, however, know this current in two limiting cases. Assuming the convolute current measurement is trustworthy and that there is no loss of current in the feed section, we can use this experimental measurement to construct the mean current radius in the array volume. Alternatively, we assume there is a current loss at the start of the feed section and monitor the current in our load calculation consistent with the convolute voltage. Taking this lower current, we can construct an alternative measure of the load inductance, hence current radius. In this respect, our two limiting cases either assume all the current reaches the array volume, or instead there is a significant current loss at the beginning of the final power feed. These two cases are compared in Fig. 9 for the 2.5 mg array implosion. For reference, we include our simulated center of mass implosion trajectory and the radii and widths of the radiographic density measurement we compared to in Fig. 4. Widths are calculated by locating the inner and outer bound of the central 50% of the mass. The second radiograph point uses the simulated rather than measured density distribution due to uncertainties in the reliability of that specific measurement. Since we are able to monitor the actual mean current radius in the simulations, this measure is also included for comparison with the inductance unfold.

In our simulations, we see that the mean current radius essentially follows the center of mass implosion trajectory.

Downloaded 18 Jan 2011 to 134.253.26.11. Redistribution subject to AIP license or copyright; see http://pop.aip.org/about/rights_and_permissions

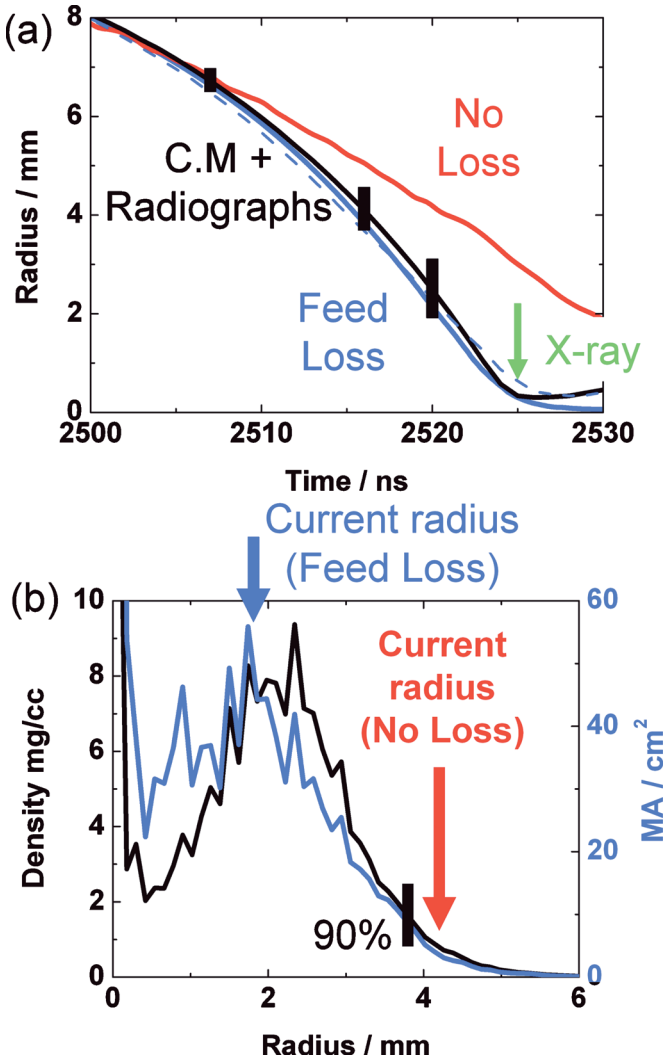

FIG. 9. (Color) (a) A 2.5 mg array implosion current trajectories. Black line: center of mass (CM) implosion trajectory with widths measured from radiographs. Red line: inductance unfold of current radius using measured convolute current (assuming no loss). Blue line: inductance unfold using calculated current (with feed loss), shown with calculated mean current radius (dotted line). (b) Density distribution matching the late time radiograph of Fig. 4(c) (black), shown with calculated current density distribution (blue). Also shown are the radius enclosing 90% of array mass and the unfolded mean current radius assuming no current loss within the final feed.

Assuming a current loss in the feed, the inductance unfold of our calculated current agrees with both of these trajectories, and with the center of mass calculated from the radiographs. This demonstrates that the inductance unfold is a reasonable measure of the mean current radius, proving self-consistency within our calculation, but also indicating that the current essentially follows the mass. Figure 9(b) compares the calculated current density distribution with the density distribution previously validated in Fig. 4(c). Current is actually seen to slightly precede the mass, driving the leading edge of the implosion.

Alternatively, if we assume there is no loss of current then the inductance unfold is seen to lag behind the implosion by ~2 mm, with current predominantly flowing outside the radius enclosing 90% of the array mass [Fig. 9(b)]. This implies another current path within the array volume that our

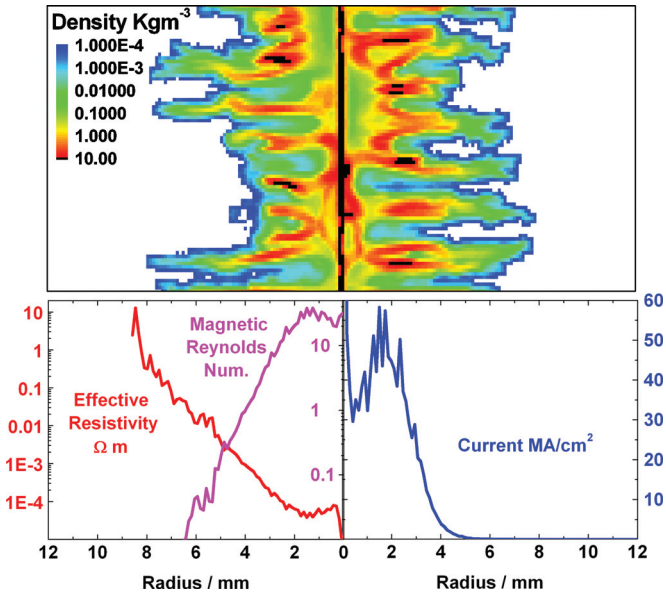

FIG. 10. (Color) Logarithmic density contour of slice through center of array ~5 ns before peak x ray. (b) Effective azimuthally and axially averaged resistivity of imploding and trailing material. (c) Radial current distribution.

simulations do not account for. This can be interpreted as current trailing behind the main implosion, but as these results demonstrate, this is also consistent with a loss of current within the power feed. Experimentally, it is difficult to differentiate between these processes, but calculations assuming a current loss have agreed with a large number of the experimental measurements. Starting from these, we can examine what is required to produce the trailing current necessary to agree with convolute current measurements. We can then determine if this is feasible and if agreement with observation can be retained through this approach.

A. Current trailing behind the main implosion

It has long been understood that some proportion of the mass is left trailing behind in the implosion of a wire array. Given the existence of low density plasma out to large radius, it seems reasonable to expect a significant amount of current to also trail the implosion, and yet such trailing current is not observed in our calculations. To fully understand why we can further interrogate the 2.5 mg array implosion, Fig. 10 shows logarithmic density contours of a slice cut through the center of the array, once again at the same time as the radiograph compared to Fig. 4(c). The penetration of MRT instabilities has left a small fraction (<5%) of the array mass trailing out to a radius of ~8 mm; however, 95% of the current is confined within a radius of 3.5 mm at this time. This indicates that our trailing mass is not conductive enough to support an appreciable fraction of the drive current. Comparing the current distribution to this density slice in Fig. 10(c), we see that the current is effectively confined to a small radius by the front of the MRT bubbles. The implosion is being driven by the current carried in the leading edge of these imploding bubbles, with the effective resistivity of the trailing mass being maintained by the gaps opened

Downloaded 18 Jan 2011 to 134.253.26.11. Redistribution subject to AIP license or copyright; see http://pop.aip.org/about/rights_and_permissions

up by the growth of these implosion instabilities. Axial current is unable to directly bridge vacuum gaps between MRT bubbles at large radius, and the inductively unfavorable current path of going to the small radius then back out again encourages the current to redirect azimuthally[31] and flow in closer proximity to the front of the implosion. These mechanisms have the effect of reducing the current flowing in the trailing mass at large radius and, in a simplistic picture, may be thought of as an enhancement to the effective resistivity of the trailing material. To quantify this effective resistivity, we can calculate the total Ohmic heating rate at a given radius and from the average axial current flowing at that radius construct an effective resistivity, which we show in Fig. 10(c) Assuming a characteristic scale length of ~ 2 mm, corresponding to the imploding shell width, we also show the effective magnetic Reynolds number as a function of radius. This is seen to drop below 1 at a radius of ~ 4 mm, so outside this radius, the magnetic field has little difficulty in diffusing through the trailing mass, allowing the current to be concentrated in the bulk of the imploding plasma. In this way, the development of implosion instabilities can be thought of as an enhancement to the resistivity of the trailing mass. Low density plasma may exist at large radius, but its effective resistivity is potentially very high. When simply regarded as a resistive medium, this presents a contradiction in requiring trailing mass left by MRT instability growth to support a trailing current. To be left behind in the first place, the plasma must be resistive enough for the magnetic field to pass through it and continue driving the implosion, yet to support several MA of trailing current, it must be conductive enough that the magnetic field cannot pass through it and is retained in this trailing material. Our simulation results are consistent with both the existence of trailing mass out to large radius and the concentration of the current to small radius. However, the MHD mechanism responsible for leaving this trailing mass is incompatible with the requirement that it then supports the trailing current.

It is conceivable that time dependant processes, such as photoionization, may increase the conductivity of this trailing material, allowing it to support additional current, but the mean current radius assuming no loss is seen to diverge from the implosion trajectory very early on, and then not respond to the main x-ray pulse. Also, since the vast majority of the mass is accounted for by the radiography, only a small percentage of the mass would be available to support this current, and so would easily be swept up into the main implosion.

Assuming, however, that some way can be found to support a conducting medium behind the main implosion that does not itself implode, we can attempt to quantify how much current this medium must support. In our calculations, we can assign a minimum conductivity to the vacuum surrounding the plasma, allowing a current to flow in the volume between the implosion front and original wire location. Continuing to drive our calculation with the known convolute voltage, we can adjust the value of this vacuum resistance until our calculated load current measurement agrees with the measured convolute current. This result is shown in Fig. 11, where a vacuum resistivity of 0.013 Ω m was found

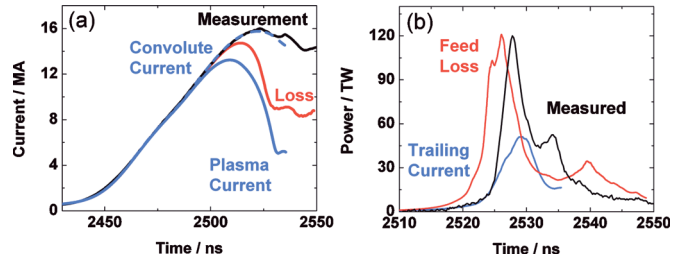

FIG. 11. (Color) (a) Blue: simulated convolute current (dashed line) and current in the plasma (solid line) assuming trailing current. Red: load current assuming current loss in the power feed. Black: measured convolute current. (b) Soft x-ray powers measured, simulated with feed loss, and simulated with trailing current.

to be required. For comparison, we also show the current now making it into the actual plasma along with the previous load current calculated, assuming a current loss in the power feed. This demonstrates that relying on the mechanism of trailing current flowing within the array volume leads to a lower current in the plasma than resulted from assuming current loss in the power feed. The x-ray power produced from this lowered drive current is also seen to be ~ 3 ns later than the feed loss calculation, and more than 50% below the experimentally measured power. It is possible that higher powers could be recovered by modifying some of the assumptions in our wire array model, such as initial perturbation amplitudes or the radiation loss model employed. However, for this comparison, the reduction in power does seem to indicate that if we assume trailing current, we are less able to couple energy to the radiating pinch, than if we assume a current loss in the power feed. The actual width of the imploding mass distribution for this trailing current case did still agree with the radiographic measurement. However, the degree of low density trailing material behind this was reduced. Reconnection of current across the MRT bubbles simply allowed this material to be accelerated into the main implosion.

B. Current loss in the feed

Given the difficulty in matching measured currents and x-ray powers using a trailing current within the array volume, we can further examine the possibility of a current loss in the power feed that connects the convolute to the array. Over the lifetime of the Z generator, a number of different feed configurations have been fielded, allowing us to compare a number of different loads and assess any dependence of the current loss on the specific nature of the power feed.

To effectively compare different final power feed configurations, we must first distinguish between current losses that are known to occur in the convolute and current losses that we now infer in the power feed. By the same translation procedures used to recover the convolute voltage, we can also recover the current entering the convolute. Convolute current measurements directly diagnose the current leaving the convolute, so these three measurements allow us to measure the convolute current lost and calculate the effective time dependent resistance of this loss. For any given wire array implosion, this provides us with an effective measure

Downloaded 18 Jan 2011 to 134.253.26.11. Redistribution subject to AIP license or copyright; see http://pop.aip.org/about/rights_and_permissions

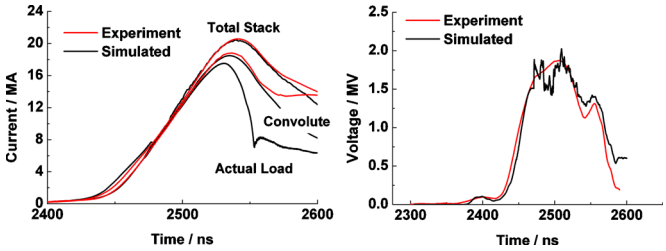

FIG. 12. (Color online) Transmission line circuit model of the Z generator including separate convolute and feed current losses. (a) Simulated and measured currents at the insulator stack and convolute, and the simulated current in the load region assuming flow impedance loss of 0.18. (b) Measured convolute voltage with simulated voltage from this circuit model, assuming additional feed current loss.

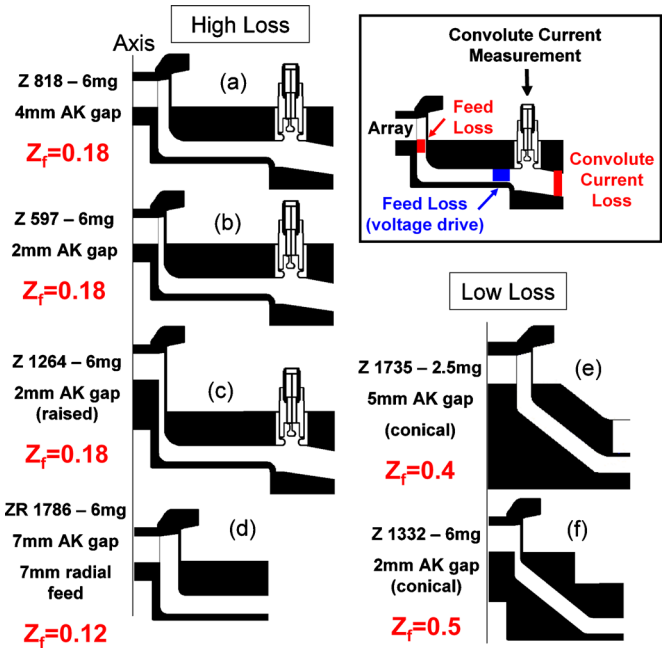

FIG. 13. (Color online) Final feed geometry and corresponding flow impedance for feed current loss required to agree with measured electrical measurements. The inset shows the location at which the convolute current loss and feed current loss are applied in the circuit model, relative to the convolute current measurement. Also shown is the effective feed loss location used in voltage drive discussed in Secs. IV A and IV B, used in gap scaling experiments by Stygar *et al.* (Ref. 21). (c) and (f) are from experiments by Bennett *et al.*, (e) fielded by Cuneo *et al.* (Ref. 17), and (d) fielded by Jones (Ref. 34).

of the convolute loss which may be included in an appropriate circuit model of the generator. This use of the electrical diagnostics removes the need to accurately model the convolute current loss, allowing us to examine additional losses between the convolute and the wire array.

This convolute loss element is included in a circuit model consisting of a four-level transmission line representation of the vacuum section and part of the water section behind the insulator stack [Fig. 1(a)]. These four lines are coupled together through a simple inductor resistor network that incorporates the convolute loss and drives a short transmission line representation of the final power feed that connects to our MHD model of the load. The details of this circuit model are discussed more extensively by Jennings *et al.*[7] This representation of the generator correctly accounts for any transmission line propagation effects and utilizes a measurement of convolute current loss specific to the shot being modeled.

Driving our load calculation with this circuit, we may now include an additional current loss element within the transmission line representation of the final feed, and adjust its value until we match the voltage, stack currents, and convolute current measurements. This additional current loss element is distinct from, and applied in addition to, the "measured" convolute loss resistance. In this way, we may parametrize the additional current loss in the power feed with a single number that may be used to simply compare different array implosions, where we can be confident we have separately accounted for the first convolute current loss. We choose to parametrize the power feed loss using an electron flow loss,[16] adjusting the effective flow impedance to match the circuit measurements. While this does not attempt to provide a physical picture of the nature of the feed loss, it does prove a simple comparative measure that is consistent with current loss mechanisms previously included in circuit models of the Z generator.[15] Figure 12(a) compares the measured stack and load currents with a now complete circuit model, incorporating both a convolute current loss and an additional feed loss, and driving a MHD representation of a 6 mg compact tungsten wire array load. Figure 12(b) compares the reconstructed convolute voltage with the voltage measured at this location in the simulation. As can be seen, the inclusion of an additional feed loss element in the circuit model recovers agreement with both the measured currents and voltages, using a loss represented by a flow impedance of 0.18.

Extending this method of quantifying the current loss, we can compare a number of equivalent wire array loads. Figure 13 shows six different configurations of the final feed geometry fielded on Z before and after its refurbishment. Figures 13(a)–13(d) and 13(f) all drive identical 6 mg, 300 wire compact tungsten wire array loads, while Fig. 13(e) was used to drive a lighter 2.5 mg array of the same dimensions and wire number. Shown with each feed configuration is the effective flow impedance (Z_f) required to provide sufficient current loss to match the measured currents and convolute voltage. From this comparison, we see that the current loss is not dependent on either the width or the height of the electrode gap approaching the load (AK gap), but is strongly dependent on the shape of the feed as the power feed is raised to the array height. Figure 13(d) employed the largest electrode gaps, but had a tightest radius of curvature at the bend in the feed and required the smallest flow impedance indicative of the largest current loss. The conical feed used in Fig. 13(f) resulted in the smallest current loss, despite having only a 2 mm electrode gap at the entrance to the array region. A higher hohlraum temperature was also recorded with this configuration indicative of a higher x-ray power generated by the array. While the total inductance of these feed geometries did vary, there is no consistent trend between the change in the feed inductance and the degree of current loss observed. But there does appear to be a consistent trend indicating that using a conical power feed to raise the feed to

Downloaded 18 Jan 2011 to 134.253.26.11. Redistribution subject to AIP license or copyright; see http://pop.aip.org/about/rights_and_permissions

the array height dramatically decreases the level of current loss. Since the wire arrays driven by five of these feed geometries were all identical, there is also little reason to believe that the wire array implosion dynamics changed significantly enough to dramatically affect current loss within the array volume. Therefore, given the strong dependence observed between the current loss and the geometry of the feed, it seems reasonable to conclude that the current loss we first inferred from the voltage measurements is associated with the power feed to the array rather than the array itself.

For these calculations where we use a circuit representation of the Z generator to drive the array implosion, the location of the current loss in the feed was chosen to be at the entrance to the array volume as indicated in the inset of Fig. 13. This differs from the effective location of the feed loss when we use the voltage drive discussed in Sec. III. Using the measured convolute voltage to drive the feed and wire array implied that the additional current loss in the feed was located in close proximity to the current loss in the convolute, separated by a negligible inductance (this loss location is also indicated in Fig. 13). This indicates that electrical data are potentially consistent with a current loss regardless of where in the feed that loss is located. Validation against array implosion and stagnation data was, however, performed using the voltage drive, and so assuming the current loss at the start of the final feed. It may be possible to use our MHD load model, constrained with all the available data, to explore how implosion results vary with the assumed location of this current loss, enabling us to better determine the exact placement and nature of this loss. Such analysis is the subject of ongoing work.

VI. PRODUCING THE POWER

Assuming our model produces the correct load dynamics (as shown in Sec. IV) and is driven with the correct current (as shown in Sec. V), we can now examine the energetics and processes responsible for x-ray production in a little more detail. Looking at the 2.5 mg array implosion studied as part of the mass scan, we can monitor the flow of energy through the system over the course of the implosion and stagnation,

$$IV = \underbrace{IR}_{1} + \underbrace{\int_V v \cdot j \times B}_{2} + \underbrace{\int_V \frac{1}{2\mu_0}\frac{\partial B^2}{\partial t}}_{3}. \tag{1}$$

The IV electrical power delivered to the load can go into one of three places, shown in Eq. (1). It can be dissipated by the total resistance (term 1), it can do work in accelerating the plasma through the $j \times B$ force (term 2), or it can supply energy to building up the magnetic field (term 3). Figure 14(a) shows how the electrical power delivered to a 2.5 mg wire array principally goes into building up the magnetic field in the load region or the kinetic energy of the plasma as it is accelerated. The resistive dissipation of this energy remains negligible. Looking specifically at the power delivered to the plasma through work done by the $j \times B$ force in Fig. 14(b), we see that over the course of the implosion, this simply goes into building up the kinetic energy of the imploding plasma as we would expect. As the plasma stagnates on axis, the rate of change of kinetic energy becomes negative, as the implosion kinetic energy is thermalized and radiated. The work done by the magnetic field through the $j \times B$ force remains positive, reaching a maximum during this time. In fact, at peak x-ray power, nearly ~75 TW of power is being delivered through this mechanism. This means that less than half of the total radiated energy is derived from kinetic energy built up during the implosion. The remaining larger contribution to the radiated power is still derived from work done accelerating the plasma and supplying kinetic energy. However, it is now being delivered by the generator circuit to the pinch during the stagnation rather than the implosion.

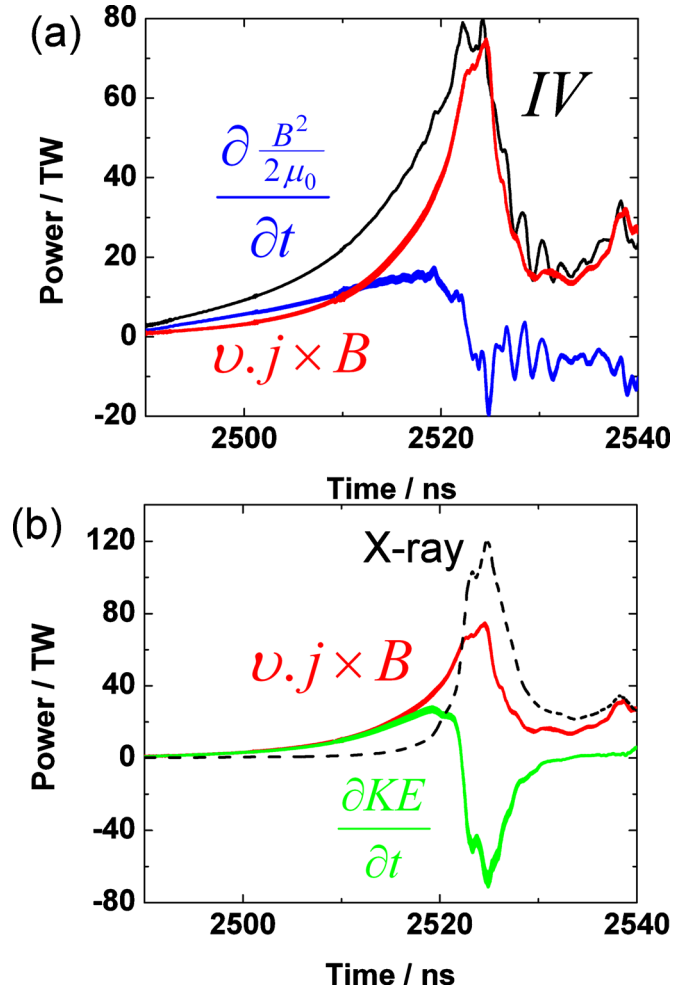

FIG. 14. (Color online) (a) IV electrical power delivered to load region, with work done on the plasma and rate of change of magnetic energy density. (b) Work done on the plasma compared to x-ray power and rate of change of kinetic energy.

In a simple representation of a wire array implosion, the wire array can be thought of as the final stage of energy pulse compression in the generator system. The generator compresses the electrical pulse discharged by the capacitor banks through a series of switches and pulse forming lines. This electrical energy then builds up the wire array kinetic energy

Downloaded 18 Jan 2011 to 134.253.26.11. Redistribution subject to AIP license or copyright; see http://pop.aip.org/about/rights_and_permissions

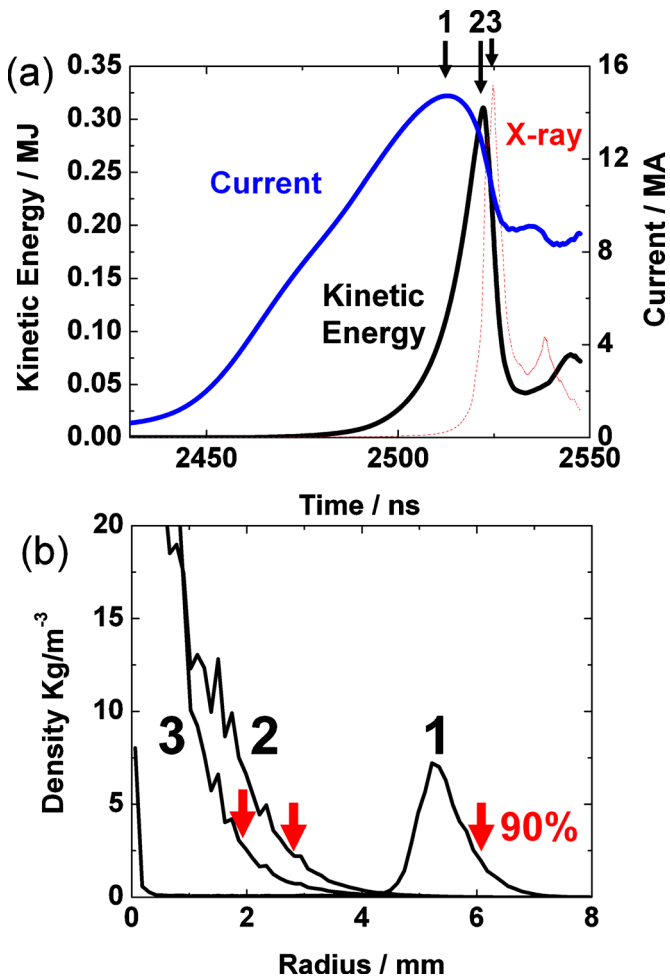

FIG. 15. (Color online) (a) Current supplied and kinetic energy delivered to the imploding pinch. (b) Radial density distributions at peak current, peak kinetic energy, and peak x ray. Arrows denote radius enclosing 90% of the mass.

over ~100 ns, and this energy is thermalized and radiated over ~2–5 ns as the array stagnates on axis. However, half the energy radiated is attributable to electrical energy delivered through the x-ray power pulse. In this respect, the wire array serves as the final stage of electrical pulse compression as well. The changing inductance of the imploding array has ultimately compressed ~100 ns electrical power pulse into the ~5 ns electrical power pulse delivered to the stagnating plasma and contributing a significant amount of the total radiated energy.

In Fig. 15(a), we show the kinetic energy of the imploding array as a function of time, alongside the current flowing through the pinch. For reference, we also show density distributions at representative times in Fig. 15(b). At peak current, the imploding mass is still at a radius of 5.4 mm, more than half the initial array radius, and only 0.1 MJ of kinetic energy has built up in the system by this time. This will go on to account for only 16% of the energy radiated in the main x-ray pulse (as defined by the energy radiated by the time the x-ray pulse has dropped to half its peak value). The current has reached its maximum and is beginning to drop in response to the rising inductance of the imploding load. The majority of both the implosion kinetic energy and total energy that will go on to be radiated is now being delivered while the load current is dropping. The maximum kinetic energy of 0.31 MJ, which still only accounts for half the energy radiated, is reached 2.5 ns before peak x ray. At this time, some of the imploding mass has stagnated on axis, while the rest of the mass distribution is still being accelerated, with the radius enclosing 90% of the array mass still seen to extend out to 3 mm. In this respect, the peak kinetic energy is not the total kinetic energy generated; instead, it is the point at which the kinetic energy lost through deceleration onto the axis equals the kinetic energy gained through acceleration of the remaining material. The kinetic energy held in the imploding plasma maximizes during the x-ray pulse, about half way up the its rise to peak. The kinetic energy then drops to its minimum value over the remainder of the x-ray pulse as the distributed mass profile assembles on axis. However, work continues to be done accelerating the remaining imploding plasma throughout this time. Indeed, it is during this prolonged stagnation that the rate at which work is done on the plasma maximizes, peaking at 75 TW at the same time as the peak x-ray power, as shown in Fig. 14(b).

Assuming resistance effects are negligible, the voltage over an imploding wire array is simply determined by its inductance. Integrating by parts the electrical power delivered to the load, we can see from Eq. (2) that this power is either delivered into the stored magnetic energy (term 1) or into work done on the plasma (term 2). It is important to note that the inductance referred to here is the flux inductance as discussed by Waisman *et al.*[22] For the cylindrical system, we discuss the inductive energy stored in term 1 may only be identified with the total energy stored in the magnetic field when we assume an infinitely thin current carrying shell. The simple representation of Eq. (2) is therefore only intended to be illustrative, rather than truly representative of the broadly distributed imploding shell we know exists,

$$\int IVdt = \underbrace{\frac{1}{2}LI^2}_{\text{Magnetic Energy}} + \underbrace{\frac{1}{2}\int I^2\dot{L}dt}_{\text{Work}}, \tag{2}$$

$$\dot{L} = \frac{\mu_0 l}{2\pi}\frac{v}{r}. \tag{3}$$

The rate at which work is done on the plasma is set by the rate of change of the inductance, which for an imploding cylindrical shell is simply set by the velocity and the radius. From this expression, it is evident that the high velocities converging to small radius found during stagnation result in the high electrical power delivered to the plasma. While Eq. (3) applied to Eq. (2) is strictly only true in the thin shell approximation, it does illustrate how kinetic energy is most rapidly built up in the plasma, as the plasma is stagnating and the current is dropping. In fact, from the calculation discussed in Fig. 15, more than ~80% of energy eventually radiated in the main x-ray pulse is delivered in the last ~20% of the implosion time. For a distributed mass profile, the implosion kinetic energy reached at the start of the x-ray

Downloaded 18 Jan 2011 to 134.253.26.11. Redistribution subject to AIP license or copyright; see http://pop.aip.org/about/rights_and_permissions

pulse as the imploding mass first begins to stagnate on axis is not representative of the total kinetic energy delivered into the plasma. As first described by Peterson *et al.*[4] for a distributed mass profile, work continues to be done accelerating some of the plasma throughout stagnation and x-ray production. We therefore cannot simply assume that most of the work is done during the implosion and that a negligible amount of additional work is done accelerating the plasma once stagnation begins. It is actually in this final stage that work is done and energy is delivered from the generator to the plasma at its greatest rate.

The implications of this late time power delivery can be more clearly demonstrated if we consider in more detail the stagnation of the 1.1 mg array, an implosion that was analyzed extensively by Sinars *et al.*[20] They noted that considering the implosion of a thin current carrying shell, the total work done in accelerating the shell depends only on the current applied and the final radius to which the implosion converges. It was found that for kinetic energy delivered in this way to be sufficient to explain the energy radiated in the main pulse, the convergence ratio of the implosion must be >30. Since direct measurements of the final pinch size demonstrated a convergence ratio of $\sim 15-20$, there existed a discrepancy. The implosion kinetic energy assessed using the final measured pinch size was found to be too low to explain the radiation yield. This same discrepancy had previously been reported on a number of z-pinch experiments.[32,33] It has been suggested that following stagnation, an additional heating mechanism was required to explain the additional energy contributing to the x-ray pulse. This separated x-ray production into the two discrete events of thermalizing the imploding kinetic energy at the observed stagnation radius, then providing additional heating to deliver energy into a dense plasma column. Examples of proposed heating mechanisms have included enhanced resistivity, additional compression (PdV work) or some form of turbulent dissipation.

Our calculation of the 1.1 mg array implosion radiates 416 kJ in the main x-ray pulse, within the errors of the 440 ± 28 kJ reported for this array. A thin shell ablation model of this implosion driven by the same current that flows in our MHD calculation [Fig. 16(a)] is indeed found to require a convergence ratio in excess of 40 to explain the energy radiated. However, in our calculation, the mean current radius (defined by the radius that encloses 50% of the current) is seen to reach ~ 0.47 mm [Fig. 16(c)] giving a convergence ratio of ~ 21, comparable to that measured for this array. This does mean that half of the current did converge to a smaller radius than this and was able to deliver energy according to this high convergence. Indeed, a convergence ratio assessed using the inductance unfold procedures discussed in Sec. V would reflect the small radius reached by a fraction of the current and imply a higher convergence ratio. This would, however, not be truly representative of the average convergence reached by a radially distributed current profile. On average, our calculation was able to maintain a large final pinch radius, yet was still able to supply sufficient energy to account for all that was radiated.

This discrepancy does highlight the difference between the stagnation of a distributed current and mass and a thin shell representation of the implosion. For a thin shell, we must continue building up kinetic energy until we account for all the radiated energy, at which point we stop the implosion at whatever radius it reached and assume that energy to be thermalized and radiated. This precludes the possibility of kinetic energy being both generated and radiated at the same time. It therefore requires our thin shell to be accelerated for an unnecessarily long time, to an unnecessarily small radius

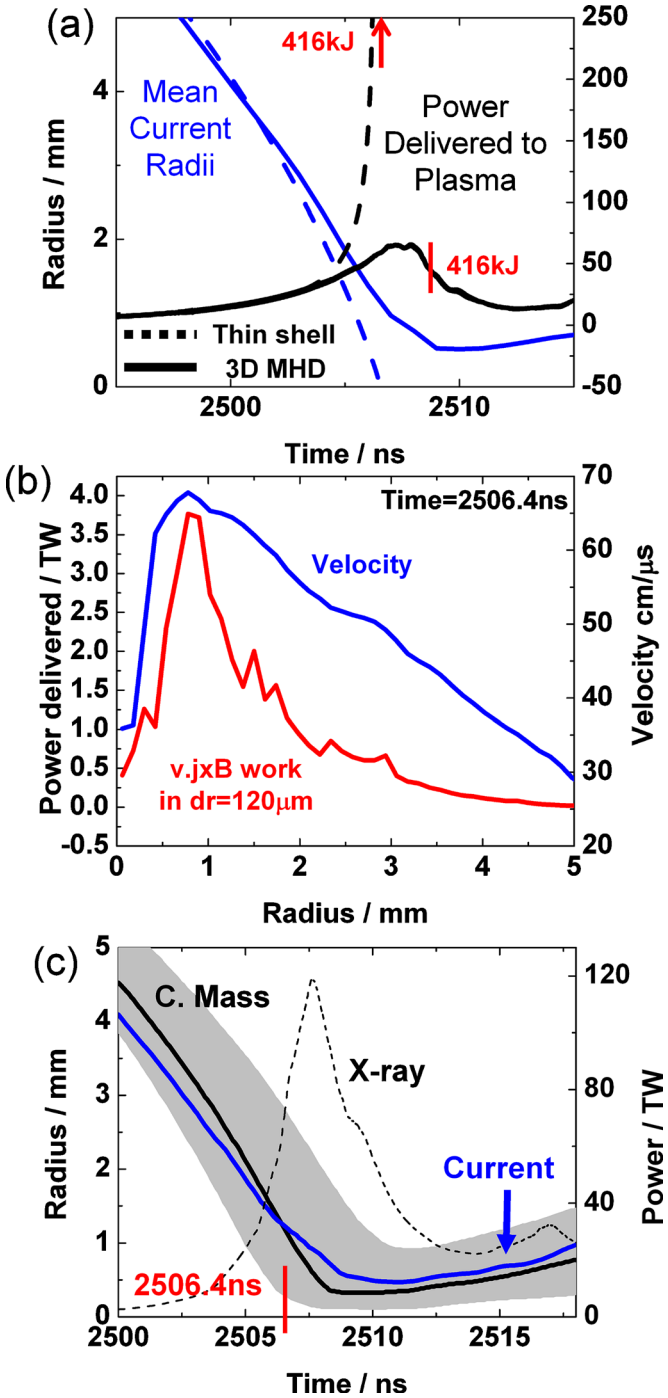

FIG. 16. (Color online) (a) Comparison of 0D current radius with MHD center of current radius, along with $v.j \times B$ work delivered into accelerating the plasma. (b) Radial distribution of $v.j \times B$ work done on the plasma with velocity distribution half way up x-ray rise time. (c) Implosion trajectory of center of mass and the radius enclosing 50% of current, with reference to x-ray pulse. The gray band indicates width of central 80% of mass.

Downloaded 18 Jan 2011 to 134.253.26.11. Redistribution subject to AIP license or copyright; see http://pop.aip.org/about/rights_and_permissions

to account for all the energy observed before we radiate it. This is demonstrated in Fig. 16(a) where we compare the mean current implosion trajectories of a thin shell ablation model with our 3D resistive MHD calculation. Also shown is the total work done accelerating the plasma ($v.j\times B$) and the point at which this power has supplied the required 416 kJ to account for the energy radiated. For the thin shell implosion, this power tends to infinity as the axis is approached. The sharp divergence of the power means that to supply additional energy in the decreasing time remaining before the axis is reached, we must integrate very high powers, allowing the pinch to converge to very small radii. Alternatively, our 3D calculations, as in the two-dimensional calculations of Peterson *et al.*,[4] take several nanoseconds during the x-ray pulse for the broad radial distribution of mass to assemble at finite radius. The power that supplies kinetic energy to the pinch remains high throughout this time, providing the required additional energy over the duration of the x-ray pulse.

To see the nature of this additional power supplied, we can look at the work done on the plasma as a function of radius. We look at a time during the x-ray pulse, half way up the rise to peak, when 50 TW of power is supplying the kinetic energy. Figure 16(b) shows the azimuthally integrated power density ($2\pi rv.j\times B$) delivered into the kinetic energy as a function of radius, which we compare with the radial velocity distribution. The peak in the power delivered is seen to coincide with the peak in velocity just before the deceleration region of the stagnation. This additional power, supplied during the x-ray pulse, is therefore simply acceleration of the mass that is still imploding, but has not yet reached the axis. Given the high velocity and small radius reached just before stagnation this power can be very high, supplying a significant fraction of the total radiated energy in the short time during which it acts. Additionally, since this work maximizes in the plasma imploding at the highest velocity, it is distinct from the work that the $j\times B$ force might do in further compressing the plasma after stagnation. It does not therefore require compression of the plasma to very small radius.

This continued acceleration of imploding plasma is aided by the current remaining at finite radius. In Fig. 16(c), we compare the implosion trajectories of the center of mass and the mean current radius. We also show the width of the central 80% of the imploding mass, denoted by the gray band, and the x-ray power pulse. This demonstrates that the width of the radiation pulse is simply set by the time taken for this wide imploding shell to stagnate. Prior to stagnation, the current precedes the center of mass, carried in the leading edge of imploding MRT bubbles. As the axis is approached, the mean current radius is seen to pull back from the mass to implode behind the center of mass during the x-ray pulse. Given the unfavorably high inductance of a current path at very small radius, the current simply seeks an alternative current path at larger radius. This is made possible by the large width of the imploding shell and the high degree of azimuthal asymmetry in a full circumference array calculation. In a mechanism described by Yu *et al.*,[31] if a MRT bubble attempts to implode the current to the axis, it may simply divert to mass at a larger radius in a different azimuthal location and implode that mass instead. Through this mechanism, the current is able to redistribute itself through the full width of the imploding shell and continue to do work accelerating this material to the axis. Importantly, this mechanism would not be recovered in a two-dimensional r-z calculation, where MRT bubbles could successfully implode current and mass to very small radius. This has the potential to produce unphysically large convergence ratios, preventing all of the shell mass from fully participating and so limiting the additional kinetic energy that may be supplied to be radiated.

Given the continued acceleration of the full width of the imploding shell, there is actually no discrepancy between the energy radiated and the radially directed kinetic energy supplied by the magnetic field doing work on the imploding plasma. We do not require any additional heating mechanisms; we simply must take account of the fact that for a broad imploding mass distribution, kinetic energy continues to be supplied throughout stagnation. The plasma does not stagnate into a stationary column that we must then heat. Instead, we have a dynamically evolving system in which kinetic energy is being thermalized and radiated while it is still being generated.

VII. SUPPLYING THE ENERGY

What is of particular interest in this process is the fact that the additional power supplied through stagnation scales as I^2 [Eq. (2)], but is being delivered while the current is dropping. The ability of the generator to deliver this energy depends less on the current that is supplied during the implosion, and more on how effectively the current can be supported through stagnation. It depends on the specific design of the generator and how it responds to the load. An array radius and mass can be selected to increase the kinetic energy delivered going into the stagnation by simply increasing the current. However, if we were to optimize our arrays based only on considering the peak current, then we are only directly attempting to optimize the first 20% of total energy delivered. Given the current loss we now accept, the true current flowing through the imploding pinch is seen to drop significantly both before and during the x-ray pulse in response to the rising inductance of the imploding array. The amount of current available to work on the plasma during this time is therefore determined by the voltage the generator is able to support at stagnation.

The voltage reaching the load is simply the voltage sourced from the generator at the convolute minus the voltage dropped over the final feed section [Eq. (4)]

$$V_{\mathrm{Load}} = V_{\mathrm{Convolute}} - L_{\mathrm{feed}}\frac{dI_{\mathrm{Load}}}{dt}. \tag{4}$$

However, since the current in the load is dropping significantly, the rate of change in current is negative, and the inductance of the feed section actually becomes the voltage source. The magnetic energy of the feed is being expended in an effort to support the dropping load current. We compare this voltage source to the voltage over the load in Fig. 17(a), where we see that around 80% of the voltage over the load is being supported just by the inductance of the feed. In this

Downloaded 18 Jan 2011 to 134.253.26.11. Redistribution subject to AIP license or copyright; see http://pop.aip.org/about/rights_and_permissions

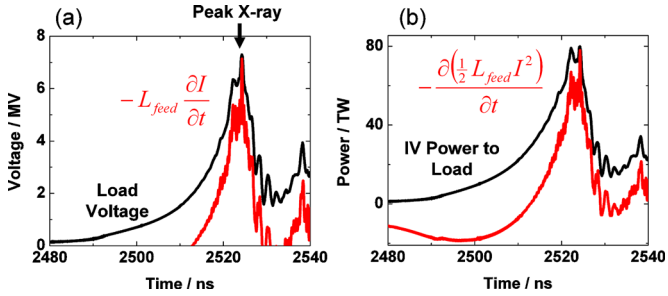

FIG. 17. (Color online) (a) Load voltage compared to voltage supported by feed inductance. (b) *IV* electrical power delivered to load compared to the rate of change of magnetic energy stored in the inductance of the feed.

respect, the *IV* electrical power supplied through stagnation, which provides a significant contribution to the radiated energy, is going to be principally drawn from the magnetic energy of the innermost sections of the power feed [Eq. (5)]. This is demonstrated in Fig. 17(b), where we compare the additional power delivered through stagnation to the rate at which magnetic energy is lost from the inductance of the feed

$$I_{\mathrm{Load}}V_{\mathrm{Load}} \approx \frac{1}{2}L_{\mathrm{feed}}\frac{dI_{\mathrm{Load}}^2}{dt}. \tag{5}$$

This is quite reasonable, in that given an x-ray power pulse <5 ns in duration, we can only effectively access energy stored within ~ 5 ft of the load. This radius encompasses much of the MITLs, but does not allow energy to be effectively sourced from either the stack or water sections which are typically associated with the effective impedance of the generator and its ability to support voltage. Additionally, given the presence of significant current losses in the vicinity of the convolute, accessing energy upstream of this location becomes more difficult, limiting the energy available to the pinch to be mainly the magnetic energy store of the final feed section approaching the array.

These results indicate that when designing wire array radiation sources for existing and future applications or generators, we should be mindful of not just how much current we can deliver during implosion, but how successfully we can support this current throughout x-ray production. For example, a late implosion of a heavy array may begin to stagnate a long time after the generators peak current. While such an array may couple more kinetic energy into the implosion, the current has already dropped as stagnation begins, meaning less magnetic energy is available in the feed inductance. The higher kinetic energy coming into the stagnation may come at the expense of kinetic energy delivered during stagnation. Since a large fraction of the radiated power comes from this energy delivered at stagnation, increasing the coupled energy with longer implosion times may not be an effective way of increasing the power. This is partly reflected in the mass scan discussed earlier where, despite the heaviest array having the greatest kinetic energy as stagnation begins, the resulting power was effectively the same as the lightest array with the lowest kinetic energy.

VIII. CONCLUSION

In this work, we have validated results from the GORGON MHD code against a broad range of experimental measurements. These have included direct measurements of wire ablation, mass profiles during stagnation, electrical data, array implosion trajectories, convergence ratios at stagnation, and radiated x-ray powers and energies. Excellent agreement is obtained with our MHD model of the implosion and this agreement allows us to infer an undiagnosed current loss in the power feed connecting the convolute to the wire array. Accounting for this loss, we are able to better assess electrical power delivery to a wire array load and demonstrate that the radiated energy is consistent with implosion kinetic energy derived from work done by the magnetic field accelerating the imploding plasma. However, a large fraction of the energy radiated by a wire array load appears to be sourced from the inductance of the hardware connecting to the load. The x-ray power radiated will therefore exhibit some dependence on the specific design of these sections of the generator, rather than simply on the peak current that can be supplied. Given a better understanding of exactly where radiated energy derives from in a wire array implosion, we can better optimize an array to a given generator, but also begin to optimize the generator for a given array. Exploring the implications of these calculations for the optimization of wire array performance and the array/generator coupling will be the subject of future work.

ACKNOWLEDGMENTS

The authors would like to thank the Z operations crew and the Z-Beamlet staff for outstanding and dedicated technical support. We are grateful for the enthusiastic programmatic support of M. K. Matzen, T. A. Mehlhorn, D. Flicker, J. L. Porter, and M. Herrmann. We also thank M. Jones for valuable conversations and for making his data available. One of the authors (C. A. Jennings) would like to particularly thank T. A. Mehlhorn for his continued support and the opportunity to pursue much of this work. This work is supported by DOE/NNSA. Sandia National Laboratories is a multi-program laboratory operated by Sandia Corporation, a wholly-owned subsidiary of Lockheed Martin Company, for the U.S. Department of Energy's National Nuclear Security Administration under Contract No. DE-AC04-94AL85000.

[1] M. K. Matzen, M. A. Sweeney, R. G. Adams, J. R. Asay, J. E. Bailey, G. R. Bennett, D. E. Bliss, D. D. Bloomquist, T. A. Brunner, R. B. Campbell, G. A. Chandler, C. A. Coverdale, M. E. Cuneo, J.-P. Davis, C. Deeney, M. P. Desjarlais, G. L. Donovan, C. J. Garasi, T. A. Haill, C. A. Hall, D. L. Hanson, M. J. Hurst, B. Jones, M. D. Knudson, R. J. Leeper, R. W. Lemke, M. G. Mazarakis, D. H. McDaniel, T. A. Mehlhorn, T. J. Nash, C. L. Olson, J. L. Porter, P. K. Rambo, S. E. Rosenthal, G. A. Rochau, L. E. Ruggles, C. L. Ruiz, T. W. L. Sanford, J. F. Seamen, D. B. Sinars, S. A. Slutz, I. C. Smith, K. W. Struve, W. A. Stygar, R. A. Vesey, E. A. Weinbrecht, D. F. Wenger, and E. P. Yu, Phys. Plasmas **12**, 055503 (2005).
[2] M. E. Cuneo, R. A. Vesey, G. R. Bennett, D. B. Sinars, W. A. Stygar, E. M. Waisman, J. L. Porter, P. K. Rambo, I. C. Smith, S. V. Lebedev, J. P. Chittenden, D. E. Bliss, T. J. Nash, G. A. Chandler, B. B. Afeyan, E. P. Yu, R. B. Campbell, R. G. Adams, D. L. Hanson, T. A. Mehlhorn, and M. K. Matzen, Plasma Phys. Controlled Fusion **48**, R1 (2006).
[3] M. E. Cuneo, E. M. Waisman, S. V. Lebedev, J. P. Chittenden, W. A. Stygar, G. A. Chandler, R. A. Vesey, E. P. Yu, T. J. Nash, D. E. Bliss, G. S. Sarkisov, T. C. Wagoner, G. R. Bennett, D. B. Sinars, J. L. Porter, W.

Downloaded 18 Jan 2011 to 134.253.26.11. Redistribution subject to AIP license or copyright; see http://pop.aip.org/about/rights_and_permissions

W. Simpson, L. E. Ruggles, D. F. Wenger, C. J. Garasi, B. V. Oliver, R. A. Aragon, W. E. Fowler, M. C. Hettrick, G. C. Idzorek, D. Johnson, K. Keller, S. E. Lazier, J. S. McGurn, T. A. Mehlhorn, T. Moore, D. S. Nielsen, J. Pyle, S. Speas, K. W. Struve, and J. A. Torres, Phys. Rev. E **71**, 046406 (2005).

[4]D. L. Peterson, R. L. Bowers, K. D. McLenithan, C. Deeney, G. A. Chandler, R. B. Spielman, M. K. Matzen, and N. F. Roderick, Phys. Plasmas **5**, 3302 (1998).

[5]R. W. Lemke, D. B. Sinars, E. M. Waisman, M. E. Cuneo, E. P. Yu, T. A. Haill, H. L. Hanshaw, T. A. Brunner, C. A. Jennings, W. A. Stygar, M. P. Desjarlais, T. A. Mehlhorn, and J. L. Porter, Phys. Rev. Lett. **102**, 025005 (2009).

[6]J. P. Chittenden, S. V. Lebedev, C. A. Jennings, S. N. Bland, and A. Ciardi, Plasma Phys. Controlled Fusion **46**, B457 (2004).

[7]C. Jennings, J. Chittenden, M. Cuneo, W. Stygar, D. Ampleford, E. Waisman, M. Jones, M. Savage, K. LeChien, and T. Wagoner, IEEE Trans. Plasma Sci. **38**, 529 (2010).

[8]S. V. Lebedev, F. N. Beg, S. N. Bland, J. P. Chittenden, A. E. Dangor, M. G. Haines, K. H. Kwek, S. A. Pikuz, and T. A. Shelkovenko, Phys. Plasmas **8**, 3734 (2001).

[9]J. P. Chittenden and C. A. Jennings, Phys. Rev. Lett. **101**, 055005 (2008).

[10]W. A. Stygar, M. E. Cuneo, R. A. Vesey, H. C. Ives, M. G. Mazarakis, G. A. Chandler, D. L. Fehl, R. J. Leeper, M. K. Matzen, D. H. McDaniel, J. S. McGurn, J. L. McKenney, D. J. Muron, C. L. Olson, J. L. Porter, J. J. Ramirez, J. F. Seamen, C. S. Speas, R. B. Spielman, K. W. Struve, J. A. Torres, E. M. Waisman, T. C. Wagoner, and T. L. Gilliland, Phys. Rev. E **72**, 026404 (2005).

[11]W. A. Stygar, R. B. Spielman, G. O. Allshouse, C. Deeney, D. R. Humphreys, H. C. Ives, F. W. Long, T. H. Martin, M. K. Matzen, D. H. McDaniel, Jr., L. P. Mix, T. J. Nash, J. W. Poukey, J. J. Ramirez, T. W. L. Sanford, J. F. Seamen, D. B. Seidel, J. W. Smith, D. M. Van DeValde, R. W. Wavrik, P. A. Corcoran, J. W. Douglas, I. D. Smith, M. A. Mostrom, K. W. Struve, T. P. Hughes, R. E. Clark, R. W. Shoup, T. C. Wagoner, T. L. Gilliland, and B. P. Peyton, Digest of Technical Papers. 11th IEEE International Pulsed Power Conference (Cat. No. 97CH36127), 1997, Vol. 1, pp. 591–596.

[12]W. A. Stygar, P. A. Corcoran, H. C. Ives, R. B. Spielman, J. W. Douglas, B. A. Whitney, M. A. Mostrom, T. C. Wagoner, C. S. Speas, T. L. Gilliland, G. A. Allshouse, R. E. Clark, G. L. Donovan, T. P. Hughes, D. R. Humphreys, D. M. Jaramillo, M. F. Johnson, J. W. Kellogg, R. J. Leeper, F. W. Long, T. H. Martin, T. D. Mulville, M. D. Pelock, B. P. Peyton, J. W. Poukey, J. J. Ramirez, P. G. Reynolds, J. F. Seamen, D. B. Seidel, A. P. Seth, A. W. Sharpe, R. W. Shoup, J. W. Smith, D. M. Van De Valde, and R. W. Wavrik, Phys. Rev. ST Accel. Beams **12**, 120401 (2009).

[13]R. B. Spielman, C. Deeney, G. A. Chandler, M. R. Douglas, D. L. Fehl, M. K. Matzen, D. H. McDaniel, T. J. Nash, J. L. Porter, T. W. L. Sanford, J. F. Seamen, W. A. Stygar, K. W. Struve, S. P. Breeze, J. S. McGurn, J. A. Torres, D. M. Zagar, T. L. Gilliland, D. O. Jobe, J. L. McKenney, R. C. Mock, M. Vargas, T. Wagoner, and D. L. Peterson, Phys. Plasmas **5**, 2105 (1998).

[14]T. C. Wagoner, W. A. Stygar, H. C. Ives, T. L. Gilliland, R. B. Spielman, M. F. Johnson, P. G. Reynolds, J. K. Moore, R. L. Mourning, D. L. Fehl, K. E. Androlewicz, J. E. Bailey, R. S. Broyles, T. A. Dinwoodie, G. L. Donovan, M. E. Dudley, K. D. Hahn, A. A. Kim, J. R. Lee, R. J. Leeper, G. T. Leifeste, J. A. Melville, J. A. Mills, L. P. Mix, W. B. S. Moore, B. P. Peyton, J. L. Porter, G. A. Rochau, G. E. Rochau, M. E. Savage, J. F. Seamen, J. D. Serrano, A. W. Sharpe, R. W. Shoup, J. S. Slopek, C. S. Speas, K. W. Struve, D. M. Van De Valde, and R. M. Woodring, Phys. Rev. ST Accel. Beams **11**, 100401 (2008).

[15]K. Struve, T. Martin, R. Spielman, W. Stygar, P. Corcoran, and J. Douglas, in Digest of Technical Papers. 11th IEEE International Pulsed Power Conference (Cat. No. 97CH36127), 1997, Vol. 1, pp. 162–167.

[16]W. A. Stygar, T. C. Wagoner, H. C. Ives, P. A. Corcoran, M. E. Cuneo, J. W. Douglas, T. L. Gilliland, M. G. Mazarakis, J. J. Ramirez, J. F. Seamen, D. B. Seidel, and R. B. Spielman, Phys. Rev. ST Accel. Beams **9**, 090401 (2006).

[17]M. E. Cuneo, D. B. Sinars, E. M. Waisman, D. E. Bliss, W. A. Stygar, R. A. Vesey, R. W. Lemke, I. C. Smith, P. K. Rambo, J. L. Porter, G. A. Chandler, T. J. Nash, M. G. Mazarakis, R. G. Adams, E. P. Yu, K. W. Struve, T. A. Mehlhorn, S. V. Lebedev, J. P. Chittenden, and C. A. Jennings, Phys. Plasmas **13**, 056318 (2006).

[18]D. B. Sinars, M. E. Cuneo, E. P. Yu, S. V. Lebedev, K. R. Cochrane, B. Jones, J. J. Macfarlane, T. A. Mehlhorn, J. L. Porter, and D. F. Wenger, Phys. Plasmas **13**, 042704 (2006).

[19]M. E. Cuneo, D. B. Sinars, G. R. Bennett, B. M. Jones, E. P. Yu, E. M. Waisman, R. M. Lemke, W. A. Stygar, M. G. Mazarakis, M. P. Desjarlais, R. A. Vesey, M. C. Herrmann, and J. L. Porter, Proceedings of the IEEE 34th International Conference on Plasma Science, ICOPS 2007, 2007, pp. 278–278.

[20]D. B. Sinars, R. W. Lemke, M. E. Cuneo, S. V. Lebedev, E. M. Waisman, W. A. Stygar, B. Jones, M. C. Jones, E. P. Yu, J. L. Porter, and D. F. Wenger, Phys. Rev. Lett. **100**, 145002 (2008).

[21]W. A. Stygar, H. C. Ives, D. L. Fehl, M. E. Cuneo, M. G. Mazarakis, J. E. Bailey, G. R. Bennett, D. E. Bliss, G. A. Chandler, R. J. Leeper, M. K. Matzen, D. H. McDaniel, J. S. McGurn, J. L. McKenney, L. P. Mix, D. J. Muron, J. L. Porter, J. J. Ramirez, L. E. Ruggles, J. F. Seamen, W. W. Simpson, C. S. Speas, R. B. Spielman, K. W. Struve, J. A. Torres, R. A. Vesey, T. C. Wagoner, T. L. Gilliland, M. L. Horry, D. O. Jobe, S. E. Lazier, J. A. Mills, T. D. Mulville, J. H. Pyle, T. M. Romero, J. J. Seamen, and R. M. Smelser, Phys. Rev. E **69**, 046403 (2004).

[22]E. M. Waisman, M. E. Cuneo, W. A. Stygar, R. W. Lemke, K. W. Struve, and T. C. Wagoner, Phys. Plasmas **11**, 2009 (2004).

[23]E. M. Waisman, M. E. Cuneo, R. W. Lemke, D. B. Sinars, and W. A. Stygar, Phys. Plasmas **15**, 042702 (2008).

[24]P. Corcoran, J. Douglas, I. Smith, P. Spence, W. Stygar, K. Struve, T. Martin, R. Spielman, and H. Ives, Digest of Technical Papers. 11th IEEE International Pulsed Power Conference (Cat. No. 97CH36127), 1997, Vol. 1, pp. 466–473.

[25]D. L. Peterson, R. L. Bowers, W. Matuska, K. D. McLenithan, G. A. Chandler, C. Deeney, M. S. Derzon, M. Douglas, M. K. Matzen, T. J. Nash, R. B. Spielman, K. W. Struve, W. A. Stygar, and N. F. Roderick, Phys. Plasmas **6**, 2178 (1999).

[26]R. W. Lemke, M. D. Knudson, A. C. Robinson, T. A. Haill, K. W. Struve, J. R. Asay, and T. A. Mehlhorn, Phys. Plasmas **10**, 1867 (2003).

[27]J. P. Chittenden, S. V. Lebedev, S. N. Bland, F. N. Beg, and M. G. Haines, Phys. Plasmas **8**, 2305 (2001).

[28]D. B. Sinars, M. E. Cuneo, E. P. Yu, D. E. Bliss, T. J. Nash, J. L. Porter, C. Deeney, M. G. Mazarakis, G. S. Sarkisov, and D. F. Wenger, Phys. Rev. Lett. **93**, 145002 (2004).

[29]D. B. Sinars, M. E. Cuneo, B. Jones, C. A. Coverdale, T. J. Nash, M. G. Mazarakis, J. L. Porter, C. Deeney, D. F. Wenger, R. G. Adams, E. P. Yu, D. E. Bliss, and G. S. Sarkisov, Phys. Plasmas **12**, 056303 (2005).

[30]M. R. Douglas, J. S. de Groot, and R. B. Spielman, Laser Part. Beams **19**, 527 (2001).

[31]E. P. Yu, M. E. Cuneo, M. P. Desjarlais, R. W. Lemke, D. B. Sinars, T. A. Haill, E. M. Waisman, G. R. Bennett, C. A. Jennings, T. A. Mehlhorn, T. A. Brunner, H. L. Hanshaw, J. L. Porter, W. A. Stygar, and L. I. Rudakov, Phys. Plasmas **15**, 056301 (2008).

[32]C. Deeney, T. J. Nash, R. B. Spielman, J. F. Seaman, G. C. Chandler, K. W. Struve, J. L. Porter, W. A. Stygar, J. S. McGurn, D. O. Jobe, T. L. Gilliland, J. A. Torres, M. F. Vargas, L. E. Ruggles, S. Breeze, R. C. Mock, M. R. Douglas, D. L. Fehl, D. H. McDaniel, M. K. Matzen, D. L. Peterson, W. Matuska, N. F. Roderick, and J. J. MacFarlane, Phys. Rev. E **56**, 5945 (1997).

[33]K. G. Whitney, J. W. Thornhill, J. P. Apruzese, J. Davis, C. Deeney, and C. A. Coverdale, Phys. Plasmas **11**, 3700 (2004).

[34]M. Jones, personal communication, 2008.

Downloaded 18 Jan 2011 to 134.253.26.11. Redistribution subject to AIP license or copyright; see http://pop.aip.org/about/rights_and_permissions